Asia Pac. J. Math. 2024 **11**:78

MODELING THE IMPACT OF CONTAMINATED ENVIRONMENTS ON THE TRANSMISSION DYNAMICS OF COVID-19 AND TYPHOID FEVER CO-INFECTION DISEASES

DANIEL S. MGONJA[1,2,*], ALFRED HUGO[1], OLUWOLE D. MAKINDE[3], ASHA HASSANI[1]

[1]Department of Mathematics and Statistics,University of Dodoma, P.O Box 259, Dodoma, Tanzania

[2]Department of Management Studies, Tanzania Institute of Accountancy, Box 9522, Dar es Salaam, Tanzania

[3]Stellenbosch University, Faculty of Military Science, Private Bagx2, Saldanba, 7395, South Africa

[*]Corresponding author: mgonja_d@yahoo.com

Received Jun. 11, 2024

Abstract. Globally, COVID-19 and Typhoid fever have posed a serious social and economic threat. This paper investigates the impact of contaminated environments on the transmission dynamics of COVID-19 and Typhoid fever co-infection using nonlinear ordinary differential equations. The model, encompassing both human and pathogen populations, undergoes analytical study, including examinations of existence, boundedness, and positivity of the solution. The next-generation matrix approach is often used to determine the basic reproduction number $\mathcal{R}_0$, and the global stability of the disease-free equilibrium point was assessed using the Lyapunov function method. Global stability analysis reveals that the disease-free equilibrium is globally asymptotically stable. Local and global stability analyses, conducted using normalized forward sensitivity indices and Partial Rank Correlation Coefficient (PRCC) methods, indicate that parameters with positive values are directly proportional to co-infected individuals. A numerical analysis of the basic reproduction number variation for various direct and indirect transmission values is conducted. The results revealed that the reduction of transmission rates and shedding rates of Typhoid fever and COVID-19 will decrease the spread of the diseases as $\mathcal{R}_0$=2.9 decreases and vice versa. Moreover, increasing hospitalization rates can effectively reduce the spread of the diseases.

2020 Mathematics Subject Classification. 92D30.

Key words and phrases. COVID-19; typhoid fever; contaminated environments; co-infection; modeling; analysis.

1. Introduction

COVID-19 and Typhoid fever, both global pandemics, exert profound impacts on health and economies worldwide [1,2]. COVID-19, caused by the highly contagious SARS-CoV-2 virus [3], induces respiratory illness and has become a pervasive global threat since its identification in Wuhan, China, in

DOI: 10.28924/APJM/11-78

2019 [2,4]. SARS-Cov-2 is a respiratory virus that transmits mainly through droplets of saliva generated from an infected person through coughing or sneezing, leading to symptoms ranging from mild to severe, including fever, cough, fatigue, and respiratory distress [3,5]. It mostly affects the lungs but can also affect other organs such as the kidneys, brain, heart blood vessels and liver [3,6].

Typhoid fever, caused by Salmonella Typhi, presents a different biological challenge in humans. Transmitted through contaminated food and water, it exclusively affects humans, manifesting symptoms such as prolonged fever, headache, vomiting, and diarrhea. It mostly affects humans' organs such as liver, spleen, gut, kidney, gallbladder and joint pains [5]. Control measures for Typhoid fever involve medical interventions like antibiotics, vaccination, and sanitation practices [7]. The disease, though potentially fatal, has not garnered the same global attention as COVID-19 [8].

Co-infection of COVID-19 and Typhoid fever adds complexity, potentially leading to severe symptoms and complicated treatment [9,10]. Individuals with Typhoid fever face an elevated risk of severe illness and death from COVID-19 [7]. The co-occurrence of symptoms makes accurate diagnosis challenging, emphasizing the importance of prompt and appropriate treatment [9,10].

The contaminated environment has a significant impact on the spread of diseases such as Typhoid fever and COVID-19 [11]. Salmonella Typhi, the bacteria that causes Typhoid fever, is commonly found in contaminated food and water [12]. It can be found in areas with low hygiene and sanitation such as, contaminated water, sources such as rivers, lakes, and wells, contaminated food, including raw fruits and vegetables washed with polluted water, as well as undercooked or raw meat and shellfish, are common surfaces of salmonella Typhi in the environment [13]. SARS-Cov-2 virus, which causes COVID-19, can be found on surfaces for varying lengths of time [14]. Some common environments where SARS-Cov-2 may be found include enclosed indoor spaces with poor ventilation where infected individuals spend time, which includes homes, workplaces, public transportation, and healthcare facilities [15]. Surfaces that are often handled by several persons, such as doorknobs, handrails, elevator buttons, blood pressure cuffs, thermometers, and stethoscopes, as well as countertops, may contain the virus if contaminated by respiratory droplets or aerosols [14].

The shedding of the pathogens from infected individuals into the environment plays a crucial role in the transmission of both Typhoid fever and COVID-19 respectively [16]. The Salmonella typhi infected individuals shed the bacteria in their feces, which can contaminate water, food sources leading to the transmission of the diseases [17]. Shedding rates of SARS-Cov-2 are particularly relevant in understanding environmental contamination and potential transmission from contaminated surfaces. Studies have shown that viable virus particles can persist on various surfaces for hours to days, depending on factors such as surface type, temperature, and humidity [18]. This environmental contamination poses a risk for indirect transmission when individuals come into contact with contaminated surfaces, and then touch their face or mucous membranes [19].

Modelling the transmission dynamics of diseases is a way to formulate what is known about the transmissions and explore all possible features of the diseases with mathematical technique [9]. The coinfection of various diseases is widely studed in the mathematical literature, for instance, Typhoid fever and cholera coinfection. COVID-19 and Dengue fever [20], these previous studies revealed that the strategies used to prevent the Dengue fever can be used to prevent the new COVID-19. COVID-19 and Cholera coinfection [21], reported that social distance and water purification as control measures can be used to prevent the spread of diseases.

However, none of these studies have explored the mathematical modeling of coinfection between COVID-19 and Typhoid fever, incorporating the impact of contaminated environment on the transmission dynamics. Therefore, this study aims to investigate the impacts of a contaminated environment on the transmission dynamics of COVID-19 and typhoid fever co-infection diseases.

2. Model Formulation

In this section, the mathematical model for the co-infection of COVID-19 and Typhoid Fever was developed. This model encompasses two main populations: the human population and the pathogen population. The human population, denoted as $N(t)$, is categorized into seven sub-classes representing various stages of susceptibility and infection. These sub-classes include the susceptible class for both Typhoid fever and COVID-19, denoted by S; the exposed class, denoted by E, representing individuals exposed to either COVID-19, Typhoid fever, or both. The infected classes were classified into three sub-classes, individuals infected with COVID-19 only, denoted by I_C; individuals infected with Typhoid fever only, denoted by I_T; individuals infected with both COVID-19 and Typhoid fever, denoted by I_{CT}; a class representing hospitalized individuals, denoted by H; and individuals who have recovered from the diseases, either naturally or through hospitalization, denoted by R.

On the pathogen side, the population is divided into two sub-classes: the concentration of Salmonella Typhi in the environment which found in contaminated food and water such as raw fruits and vegetable, raw meat and seafood, sewage and rivers, denoted by B_T, and the concentration of SARS-Cov-2 viruses in the environment which found in enclosed indoor spaces, high-touch surfaces such as doorknobs, handrails and elevator buttons, denoted by B_C. With these in mind, the expressions for the humans population and pathogens population are as follows:

$$N(t) = S(t) + E(t) + I_T(t) + I_C(t) + I_{CT}(t) + H(t) + R(t), \quad \text{and} \quad P(t) = B_T(t) + B_C(t) \tag{1}$$

In this model, it is assumed that the susceptible class increases by birth or immigration at a constant rate Λ, and also from recovered class by losing temporary immunity with α rate [10, 22]. All humans' population in each compartment suffers from natural death rate μ_1. Susceptible individuals in S acquire

Typhoid fever and COVID-19 and join the exposed class E, through contacts with infected individuals and contaminated environment by the force of infection denoted by λ.

where

$$\lambda = \lambda_1 + \lambda_2 + \lambda_3 + \lambda_4 \tag{2}$$

The susceptible individuals acquire Typhoid fever through contact with active Typhoid fever patients, co-infected patients and through contaminated environment contains salmonella Typhi, by the force of infections λ_1 and λ_2 given by:

$$\lambda_1 = \beta_1(I_T + I_{CT}) \quad \text{and} \quad \lambda_2 = \frac{\beta_2 B_T}{B_T + K_T} \tag{3}$$

In this expression, β_1 denotes the effective contact rate for Typhoid fever infection (person to person) transmission and β_2 denotes the effective contact rate due to contaminated environment (environment to person) transmission and K_T is the carrying capacity for Salmonella typhi. The susceptible individuals acquire COVID-19 through contact with individuals infected by COVID-19, co-infected patients and through contaminated environment contains SARS-Cov-2, by the force of infections λ_3 and λ_4, given by

$$\lambda_3 = \beta_3(I_C + I_{CT}) \quad \text{and} \quad \lambda_4 = \frac{\beta_4 B_C}{B_C + K_C} \tag{4}$$

In this expression, β_3 denotes the effective contact rate for COVID-19 infection (person to person) transmission and β_4 denotes the effective contact rate due to contaminate environment (environment to person) transmission and K_C is the carrying capacity for SARS-CoV-2 virus. Moreover, it is assumed that, all individuals in the exposed class undergo double screening to identify the individuals who acquire Typhoid fever only at the rate of n, COVID-19 only at the rate of m, co-infection individuals at the rate of $(n + m)$ and moves to individuals infected with COVID-19 I_C, individuals infected with Typhoid fever only I_T and individuals infected with both COVID-19 and Typhoid fever I_{CT} respectively with a transition rate of τ per day. The individuals infected by Typhoid fever or COVID-19 only, recover naturally at the rate of Ψ_1 and Ψ_3 respectively or through hospitalization, H.

It is assumed that the number of infected individuals in the classes I_C and I_T reduces through hospitalization at the transition rates of k_1 and k_3, but also through induced death at the rates of r_1 and r_3 respectively. In compartment I_{CT}, the population decreases when a fraction of that compartment recovers naturally at a rate of σ, from COVID-19 or typhoid fever, represented by h_1 and h_2, or from a fraction of co-infection that required hospitalization, represented by $(1 - (h_1 + h_2))$ at a transfer rate of k_2, and induced death rate r_2 respectively. Hospitalized individuals recovered at the rate Ψ_2 and move to the recovery class. Finally, the individuals in the R compartment reduce when return to the susceptible S state due to loss of immunity at the rate of α. Additionally, in the pathogen environment, the population decreases due to decay rates of μ_3 for Salmonella Typhi and μ_2 for SARS-CoV-2 virus, respectively. Furthermore, the Salmonella Typhi and SARS-Cov-2 increases at a growth

rates of $\rho_1 = g_T B_T(1 - \frac{B_T}{K_T})$ and $\rho_2 = g_C B_C(1 - \frac{B_C}{K_C})$ and also its growth are enhanced by Typhoid fever, COVID-19 infected individuals and co-infected individuals that are shedding into environment at the rates of g_1, g_2, g_3 and g_4 respectively.

The schematic diagram in Figure 1 is a representation of the model. The dashed arrow indicates contamination of the environment by infected humans. The dynamics of the disease can be described

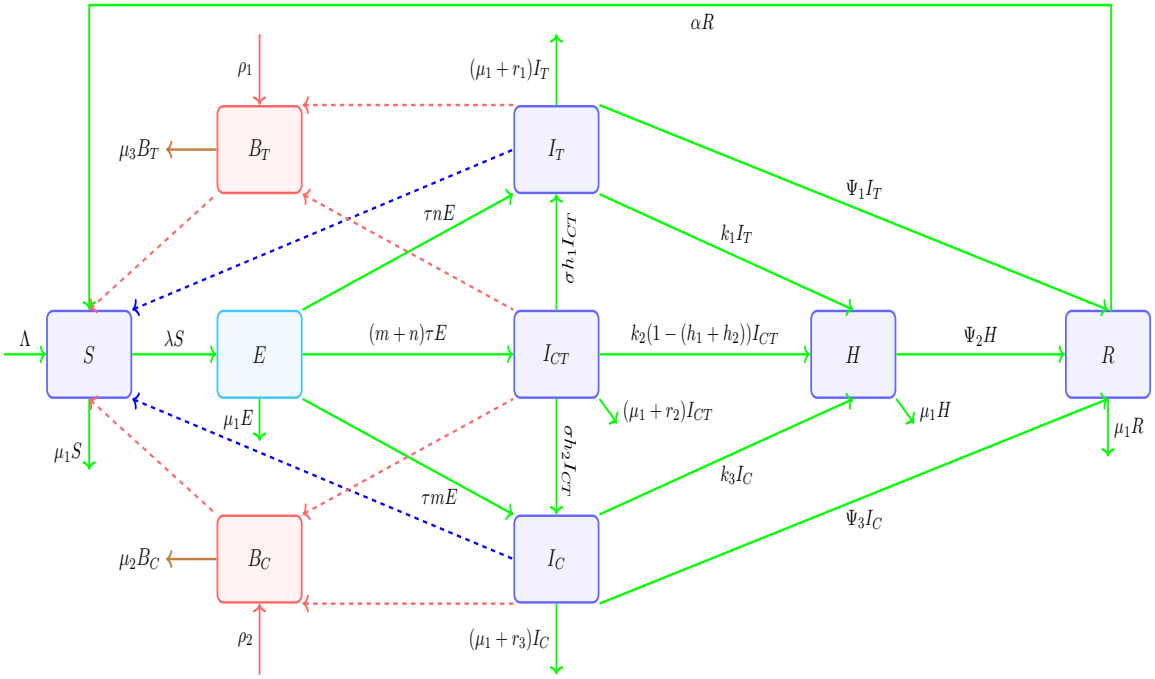

FIGURE 1. The transimmision dynamics of Typhoid fever and COVID-19 co-infection

by the following system of non-linear differential equations (5):

$$\left.\begin{aligned}
S' &= \alpha R - \lambda S - \mu_1 S + \Lambda,\\
E' &= \lambda S - (\mu_1 + \tau) E,\\
I_T' &= \tau n E + \sigma h_1 I_{CT} - (k_1 + \Psi_1 + \mu_1 + r_1) I_T,\\
I_C' &= \tau m E + \sigma h_2 I_{CT} - (\mu_1 + r_3 + k_3 + \Psi_3) I_C,\\
I_{CT}' &= (m + n)\tau E - (\sigma h_1 + \sigma h_2 + k_2(1 - (h_1 + h_2) + \mu_1 + r_2)) I_{CT},\\
H' &= k_2(1 - (h_1 + h_2)) I_{CT} + k_1 I_T + k_3 I_C - (\Psi_2 + \mu_1) H,\\
R' &= \Psi_2 H + \Psi_3 I_C + \Psi_1 I_T - (\alpha + \mu_1) R,\\
B_T' &= g_T B_T \left(1 - \frac{B_T}{K_T}\right) + g_1 I_T + g_2 I_{CT} - \mu_3 B_T,\\
B_C' &= g_C B_C \left(1 - \frac{B_C}{K_C}\right) + g_3 I_{CT} + g_4 I_C - \mu_2 B_C,
\end{aligned}\right\} \tag{5}$$

with initial conditions

$S(0) > 0$, $E(0) \geq 0$, $I_T(0) \geq 0$, $I_C(0) \geq 0$, $I_{CT}(0) \geq 0$, $H(0) \geq 0$, $R(0) \geq 0$, $B_T(0) \geq 0$ and $B_C(0) \geq 0$.

Table 1 provides the description of variables, and Table 2 are the parameters used in the proposed model.

TABLE 1. Variables of the co-infection model of typhoid fever and COVID-19

Symbol	Description
$N(t)$	The total human population N at time t
S	Susceptible human population to both COVID-19 and Typhoid Fever which is likely to be infected
E	Number of individuals Exposed to COVID-19, Typhoid fever, and co-infection.
I_T	Individuals infected with Typhoid fever only
I_C	Individuals infected with COVID-19 only
I_{CT}	Individuals infected with both Typhoid Fever and COVID-19
H	Hospitalized individuals infected with Typhoid Fever, COVID-19, and Co-infections
R	Individuals recovered from Typhoid Fever, COVID-19, and Co-infection
B_T	The concentration of Salmonella Typhi bacteria in the environment
B_C	The concentration of SARS-CoV-2 viruses in the environment

TABLE 2. Description of model parameters with units for the proposed model.

Par.	Description	Units
Λ	Constant human recruitment rate.	—
β_1	Human-to-human Typhoid fever transmission rate.	—
β_2	Environment with Salmonella typhi-to-human transmission rate.	cells^{-1}.day^{-1}.
β_3	Human-to-human COVID-19 transmission rate.	day^{-1}.
β_4	Environment with SARS-COV-2-to-human transmission rate. in the contaminated environment.	cells^{-1}.day^{-1}.
α	Rate of loosing immunity for recovered humans.	day^{-1}.
μ_1	Natural death rate of humans.	day^{-1}.
μ_2	Decay rate of SARS-COV-2 virus.	cells.day^{-1}.
μ_3	Decay rate of Salmonella typhi.	cells.day^{-1}.
k_1	The transfer rate of individuals infected by Typhoid fever only.	individuals.day^{-1}.
k_2	The transfer rate of individuals infected by Typhoid fever and COVID-19.	individuals.day^{-1}.
k_3	The transfer rate of individuals infected by COVID-19 only.	individuals.day^{-1}.
g_1	Shedding rate of Salmonella typhi by Typhoid fever infected humans.	cells.individual^{-1}.day^{-1}.
g_2	Shedding rate of Salmonella typhi by co-infected humans.	day^{-1}.
g_3	Shedding rate of SARS-COV-2 by co-infected humans.	cells.individual^{-1}.day^{-1}.
g_4	Shedding rate of SARS-COV-2 by covid-19 infected humans.	cells.individual^{-1}.day^{-1}.
r_1	Typhoid fever induced death rate.	individuals.day^{-1}.
r_2	co-infection induced death rate.	individuals.day^{-1}.
r_3	COVID-19 induced death rate.	individuals.day^{-1}.
σ	Natural recovery rate of one disease from the co-infections.	individuals.day^{-1}.
h_1	Fraction of co-infected individuals who naturally recovered from COVID-19.	day^{-1}.
h_2	Fraction of co-infected individuals who naturally recovered from Typhoid fever.	day^{-1}.
$1-(h_1+h_2)$	Fraction of co-infected individuals who attended the hospital	day^{-1}.
τ	Transition rate per day to infected classes.	day^{-1}.
m	The rate of screening for exposed individuals with COVID-19 disease.	day^{-1}.
n	The rate of screening for exposed individuals with Typhoid fever.	day^{-1}.
$(m+n)$	The rate of screening for exposed individuals with co-infection diseases	day^{-1}.
g_T	Growth rate of Salmonella typhi bacteria.	cells.day^{-1}.
g_C	Growth rate of SARS-COV-2 virus .	cells.day^{-1}.
$\Psi_1,\ \Psi_3$	Natural recovery rates for Typhoid fever, and COVID-19 respectively.	day^{-1}.
Ψ_2	Recovery rate of hospitalized individuals.	day^{-1}.
$K_T,\ K_C$	Carrying capacity for Salmonella typhi and SARS-COV-2 virus, respectively.	cells.

3. Mathematical Analysis of the Proposed Model

3.1. **Positivity and Boundedness.** Since system (5) represents the population in each class and all model parameters are all positive, then it lies in a region Ω defined by

$$\Omega = \Omega_H \times \Omega_P \in \mathbb{R}_+^7 \times \mathbb{R}_+^2 = \mathbb{R}_+^9, \text{ where}$$

$$\Omega_H = \left\{ \begin{bmatrix} S(t) \\ E(t) \\ I_T(t) \\ I_C(t) \\ I_{CT}(t) \\ H(t) \\ R(t) \end{bmatrix} \in \mathbb{R}_+^7 \middle| \begin{matrix} S(t) > 0, \\ E(t) \geq 0, \\ I_T(t) \geq 0, \\ I_C(t) \geq 0, \\ I_{CT}(t) \geq 0, \\ H(t) \geq 0, \\ R(t) \geq 0. \end{matrix} \right\}, \quad \text{and} \quad \Omega_P = \left\{ \begin{bmatrix} B_T(t) \\ B_C(t) \end{bmatrix} \in \mathbb{R}_+^2 \middle| \begin{matrix} B_T(t) \geq 0, \\ B_C(t) \geq 0. \end{matrix} \right\}.$$

For the model (5) to be mathematically and biologically meaningful, it is necessary to prove that, its solutions are all positive if their initial values are non-negative. In this subsection, the study investigates the positivity of the solution of the model and establish their bounds.

3.1.1. *Positivity of the Solution of the Model.*

Theorem 3.1. *The solutions of the model (5) are positive in the region Ω if its initial values are non-negative for all $t \geq 0$.*

Proof. Consider the ordinary differential equation for susceptible human S of the model (5),

$$\frac{dS}{dt} = \Lambda + \alpha R - (\lambda + \mu_1)S \geq -(\lambda + \mu_1)S,$$

and observe that

$$\frac{dS}{dt} \geq -(\lambda + \mu_1)S. \tag{6}$$

Upon separating variables and integrating (6), lead to

$$S(t) \geq S_(0)e^{-\int_0^t (\lambda(t)+\mu_1)dt} \geq 0.$$

By the same process, gives

$$E(t) \geq E(0)e^{-(\tau+\mu_1)t} \geq 0, \quad I_T(t) \geq I_T(0)e^{-(r_1+k_1+\Psi_1+\mu_1)t} \geq 0, \quad I_C(t) \geq I_C(0)e^{-\int_0^t (\mu_1+r_3+k_3+\Psi 3)t} \geq 0,$$

$$I_{CT}(t) \geq I_{CT}(0)e^{-(r_2+\sigma+k_2+\mu_1)t} \geq 0, \quad H(t) \geq H(0)e^{-(\Psi_2+\mu_1)t} \geq 0,$$

$$R(t) \geq R(0)e^{-\mu_1 t} \geq 0, \quad B_T(t) \geq B_T(0)e^{-\mu_3 t} \geq 0 \text{ and } \quad B_C(t) \geq B_C(0)e^{-\mu_2 t} \geq 0.$$

This implies that all solutions of the model (5) are positive for all $t \geq 0$. This ends the proof of Theorem 3.1. □

3.1.2. *Boundedness of the Model's Solutions.* The boundedness of the solutions of the model (5) on the region Ω is shown by considering the total rate of change of human population $\frac{dN}{dt}$ governed by

$$\frac{dN}{dt} = \frac{dS}{dt} + \frac{dE}{dt} + \frac{dI_T}{dt} + \frac{dI_C}{dt} + \frac{dI_{CT}}{dt} + \frac{dH}{dt} + \frac{dR}{dt} = \Lambda - \mu_1 N,$$

and observe that

$$\frac{dN}{dt} \leq \Lambda - \mu_1 N. \tag{7}$$

Using Birkhoff and Rota's theorem [23] on differential inequalities, the method of separation of variables on the inequality (7) and upon substitution of the initial conditions, gives

$$N(t) \leq \frac{\Lambda}{\mu_1} + (N(0) - \frac{\Lambda}{\mu_1})e^{-\mu_1 t}. \tag{8}$$

As $t \to \infty$, enequality (8) reduces to

$$N(t) \leq \frac{\Lambda}{\mu_1},$$

Since human population is non negative, implies that

$$0 \leq N(t) \leq \frac{\Lambda}{\mu_1}.$$

Similarly, the rate of change in Salmonella Typhi concentration in the environment produces

$$\frac{dB_T}{dt} \leq g_T B_T \left(1 - \frac{B_T}{K_T}\right) + (g_1 + g_2)\frac{\Lambda}{\mu_1} - \mu_3 B_T \tag{9}$$

If $B_T \geq \frac{(g_1+g_2)\Lambda}{\mu_1}$, then

$$\frac{dB_T}{dt} \leq (g_1 - \mu_3)B_T - \frac{g_T}{K_T}B_T^2 + B_T \tag{10}$$

This yields

$$(g_1 - \mu_3)B_T \left(1 - \frac{g_T B_T}{K_T(g_T - \mu_3 + 1)}\right) \tag{11}$$

The constant

$$\frac{K_T(g_T - \mu_3 + 1)}{g_T} \tag{12}$$

is the upper bound for the differential inequality (11) since Equation (11) is the logistic growth model with carrying capacity (12). For some $t \geq 0$, $\frac{(g_1+g_2)\Lambda}{\mu_1}$ is an upper bound for B_T where equation (10) is false, while B_T is bounded above by equation (12) for the rest of the time points in the domain B_T if equation (10) is true. The constant $\frac{(g_1+g_2)\Lambda}{\mu_1}$ is the maximum shedding rate from the Typhoid fever infected individuals. In both cases

$$B_T \leq \max\left\{\frac{K_T(g_T - \mu_3 + 1)}{g_T}, \frac{(g_1 + g_2)\Lambda}{\mu_1}\right\} \tag{13}$$

Within the feasible region

$$\Omega = \{S, E, I_T, I_C, I_{CT}, H, R, B_T, B_C\} \in \mathbb{R}_+^9 \,|\, 0 \leq N \leq \frac{\Lambda}{\mu_1},$$
$$B_T \in \left[0, \max\left\{\frac{K_T(g_T - \mu_3 + 1)}{g_T}, \frac{(g_1 + g_2)\Lambda}{\mu_1}\right\}\right],$$
$$B_C \in \left[0, \max\left\{\frac{K_C(g_C - \mu_2 + 1)}{g_C}, \frac{(g_3 + g_4)\Lambda}{\mu_1}\right\}\right] \tag{14}$$

In conclussion, the solutions of the developed model are bounded on the positive region $\Omega \in \mathbb{R}_+^9$. In this case, the developed model is mathematically and biologically meaningful and considering it for further analysis.

3.2. **Equilibrium Points and the Basic Reproduction Number $\mathcal{R}_0$.**

3.2.1. *Disease Free Equilibrium Point (DFE).* A disease-free equilibrium point (disease-free state or disease-free steady state) refers to a state in which a community or population or system is entirely free from the COVID-19 and Typhoid fever diseases. In order to analyze the disease-free equilibrium point, it is necessary to look at both the conditions necessary for its formation and the elements that contribute to the absence of disease transmission.

The DFE is established by setting the right hand side of the model system (5) to zero and substituting zero values of infectious states and the force of infection (i.e $E = I_T = I_C = I_{CT} = H = R = B_T = B_C = \lambda = 0$).

Upon solving and simplification of the resulting system, lead to

$$\text{DFE} = (S, E, I_T, I_C, I_{CT}, H, R, B_T, B_C) = \left(\frac{\Lambda}{\mu_1}, 0, 0, 0, 0, 0, 0, 0, 0\right), \text{ respectively.}$$

The formulated DFE is used to compute a state where there is no causative agents of COVID-19, Typhoid fever or both. Furthermore, DFE is used to compute the basic reproduction number $\mathcal{R}_0$ of the COVID-19 and Typhoid fever co-infection, that describes the persistence or extinction of the disease(s) within the population.

3.2.2. *The Basic Reproduction Number $\mathcal{R}_0$.* Basic reproduction number, $\mathcal{R}_0$ is a very important quantity in analyzing epidemiological models for disease control [24]. Epidemiologists can analyze the potential impact of an outbreak and forecast its future course by estimating $\mathcal{R}_0$ which provides the interpretations as follows; when $\mathcal{R}_0 < 1$, then the average number of secondary infections generated by a single primarily infected individual is less than the unity value, and hence, the disease dies out from the population. Similarly, $\mathcal{R}_0 = 1$ shows the threshold value, whereby the average number of secondary infected individuals generated by the primary infected one is constant in proportion therefore, the disease dies as well. On the other hand, if $\mathcal{R}_0 > 1$, then the number of secondary infected individuals

produced by a single primarily infected one is greater than the unity value hence, the disease will become pandemic in the entire population.

Adopting the next-generation matrix approach by [24,25] to formulate the formula for $\mathcal{R}_0$ of the model (5) is given by

$$\mathcal{R}_0 = l_{11} = R_{TH} + R_{CH} + R_{TCH} + R_{BTH} + R_{BCH},$$

where

$$R_{TH} = \frac{\beta_1 \Lambda \tau \ (\sigma \, b_1 h_1 + n a_4)}{\mu_1 a_2 a_4 a_1}, R_{CH} = \frac{\beta_3 \Lambda \tau \ (\sigma \, b_1 h_2 + m a_4)}{\mu_1 a_3 a_4 a_1}, R_{TCH} = \frac{(\beta_1 + \beta_3) \, \Lambda \, b_1 \tau}{\mu_1 a_1 a_4},$$

$$R_{BTH} = \frac{\beta_2 \Lambda \tau \ (\sigma \, b_1 g_1 h_1 + n a_4 g_1 + a_2 b_1 g_2)}{K_T \mu_1 a_2 a_4 a_1 a_6}, R_{BCH} = \frac{\beta_4 \Lambda \tau \ (\sigma \, b_1 g_4 h_2 + m a_4 g_4 + a_3 b_1 g_3)}{K_C \mu_1 a_3 a_4 a_1 a_7}.$$

By inspection, observing that, $\mathcal{R}_0$ depends on sub basic reproduction numbers; R_{TH}, R_{CH}, R_{TCH}, R_{BTH} and R_{BCH}, which respectively define the expected number of newly infected individuals produced by one infected Typhoid fever, COVID-19 and co-infection person, secondary number of infected Typhoid patients generated by ingesting salmonella typhi shed by one infected Typhoid individual, and secondary number of infected COVID-19 patients generated by ingesting SARS-COV-2 shed by one infected COVID-19 individual.

3.2.3. *Global Stability of Disease Free Equilibrium* (*DFE*). The system's long-term behavior is what determines whether the disease-free state is stable and will last over time. This behavior is referred to as the global stability of the disease-free equilibrium point. Global stability is the ability of a system to finally converge to and maintain the disease-free equilibrium point, irrespective of the system's initial circumstances or perturbations. The goal of global stability analysis is to determine whether a population will remain disease-free continuously if it begins the process without external influences like the return of an infection or changes in population dynamics. Additionally, global stability of DFE it provides insight into how well control measures will work to stop the disease's recurrence or its replication.

Theorem 3.2. *DFE is globally asymptotically stable whenever* $\mathcal{R}_0 < 1$ *as* $t \to \infty$ *and unstable otherwise.*

Proof. Let the infectious stats of the system (5) be denoted by

$$P = (E(t), I_T(t), I_C(t), I_{CT}(t), H(t), B_T(t), B_C(t))^{\mathrm{T}}.$$

Adopting the comparison principle by [26] lead to:

$$P \leq (F - V)P, \tag{15}$$

where matrices F and V are evaluated at disease-free equilibrium and $P = (E^{'}, I_T^{'}, I_C^{'}, I_{CT}^{'}, H^{'}, B_T^{'}, B_C^{'})^{\mathrm{T}}$ is a vector containing the rate of change of infected states, where

$$\left.\begin{aligned}
E^{'} &= \lambda\, S - (\mu_1 + \tau)\, E,\\
I_T^{'} &= \tau\, nE + \sigma\, h_1 I_{CT} - (k_1 + \Psi_1 + \mu_1 + r_1)\, I_T,\\
I_C^{'} &= \tau\, mE + \sigma\, h_2 I_{CT} - (\mu_1 + r_3 + k_3 + \Psi_3)\, I_C,\\
I_{CT}^{'} &= (m+n)\,\tau\, E - (\sigma\, h_1 + \sigma\, h_2 + k_2\,(1 - (h_1 + h_2) + \mu_1 + r_2))\, I_{CT},\\
H^{'} &= k_2\,(1 - (h_1 + h_2))\, I_{CT} + k_1 I_T + k_3 I_C - (\Psi_2 + \mu_1)\, H,\\
B_T^{'} &= g_T B_T \left(1 - \tfrac{B_T}{K_T}\right) + g_1 I_T + g_2 I_{CT} - \mu_3 B_T,\\
B_C^{'} &= g_C B_C \left(1 - \frac{B_C}{K_C}\right) + g_3 I_{CT} + g_4 I_C - \mu_2 B_C,
\end{aligned}\right\} \tag{16}$$

Applying the Perron-Frobenius theorem [27] for metzler matrices F and V^{-1}. Observing that $V^{-1}F$ has a dominant eigenvalue $\mathcal{R}_0 = \rho(V^{-1}F) = \rho(FV^{-1})$ that is corresponding to a non negative vector $\mathbf{a}$. It follows that $\mathbf{a}^{\mathrm{T}}V^{-1}F = \mathcal{R}_0\mathbf{a}^{\mathrm{T}}$. Motivated by [28], using Lyapunov function:

$$f(t) = \mathbf{a}^{\mathrm{T}}V^{-1}P. \tag{17}$$

Differentiating the function (17) with respect to t along with infected states of the system (5) as well as using equation (15) lead to:

$$\dot{f} = \mathbf{a}^{\mathrm{T}}V^{-1}P \leq \mathbf{a}^{\mathrm{T}}V^{-1}(F - V)P = (\mathcal{R}_0 - 1)\mathbf{a}^{\mathrm{T}}P, \text{ where } \mathbf{a}^{\mathrm{T}}P \geq 0.$$

The stability criteria $\dot{f} = (\mathcal{R}_0 - 1)\mathbf{a}^{\mathrm{T}}P \leq 0$ is attained only for $\mathcal{R}_0 < 1$.
If $\dot{f} = 0$ for $\mathcal{R}_0 < 1$, then $\mathbf{a}^{\mathrm{T}}P = 0$. Because the Perron–Frobenius eigenvector $\mathbf{a}$ has non-negative elements, then

$$P = (E, I_T, I_C, I_{CT}, H, B_T, B_C) = (0, 0, 0, 0, 0, 0, 0). \tag{18}$$

Substituting the coordinates of (18) to the model (5), gives the DFE $E_0 = (\frac{\Lambda}{\mu_1}, 0, 0, 0, 0, 0, 0, 0, 0)$.

When $\dot{f} < 0$, implies that, the infected variables I_T, I_C, I_{CT}, H, B_T and B_C loose their energy to transmit the disease to others, and therefore the system turns to DFE as $t \to \infty$. The two scenarios suggests that, every solution of the system (5) converges to DFE as $t \to \infty$ for $\mathcal{R}_0 < 1$. By LaSalle's invariant principle [29], DFE is globally asymptotically stable whenever $\mathcal{R}_0 < 1$. □

3.2.4. *Global Stability of Endemic Equilibrium E_1.* The endemic equilibrium E_1 is a state where Salmonella typhi and SARS-Cov-2 infections persists among individuals. During endemic state,the infected individuals and pathogens transmit the diseases to susceptible individuals and therefore,the number of infected individuals remains relatively constant over time.That is,the forces of infections λ_1,λ_2,λ_3 and $\lambda_4 \neq 0$. The endemic equilibrium is said to be globally stable, if in a short or long run, the disease

becomes endemic (does not die out). During this state, any invariant set in Ω close to E_1 remain close to it and eventually converges to E_1 over the indefinite time.

Definition 3.1. *A function V_x is called a Lyapunov function if it is continuous and differentiable for all values of $x \in U$ satisfying the conditions: $(i)V(x) = 0$ $(ii)V(x) > 0 \forall x \in U - (0)$ and $(iii)V'(x) \leq 0 \forall x \in U - (0)$*

Theorem 3.3. *The endemic equilibrium E^* of the model system (5) is globally asymptotically stable if the reproduction number $\mathcal{R}_0 > 1$. To prove theorem (3.3) we adopt the approach in Osman et al (2020) by concerdering the non-linear function.*

$$\begin{aligned} X =& S^* \left[\frac{S}{S^*} - \ln\left(\frac{S}{S^*}\right)\right] + E^* \left[\frac{E}{E^*} - \ln\left(\frac{E}{E^*}\right)\right] + I_T^* \left[\frac{I_T}{I_T^*} - \ln\left(\frac{I_T}{I_T^*}\right)\right] \\ &+ I_C^* \left[\frac{I_C}{I_C^*} - \ln\left(\frac{I_C}{I_C^*}\right)\right] + I_{CT}^* \left[\frac{I_{CT}}{I_{CT}^*} - \ln\left(\frac{I_{CT}}{I_{CT}^*}\right)\right] + H^* \left[\frac{H}{H^*} - \ln\left(\frac{H}{H^*}\right)\right] \\ &+ R^* \left[\frac{R}{R^*} - \ln\left(\frac{R}{R^*}\right)\right] + B_T^* \left[\frac{B_T}{B_T^*} - \ln\left(\frac{B_T}{B_T^*}\right)\right] + B_C^* \left[\frac{B_C}{B_C^*} - \ln\left(\frac{B_C}{B_C^*}\right)\right] \end{aligned} \tag{19}$$

It can be observed that the function X in (i) in the definition above for all $x \geq 0$ where $x = S, E, I_T, I_C, I_{CT}, H, R, B_T, B_C$ and x^* is the endemic equilibrium. Hence, a function X is a Lyapunov function.

To prove if condition (iii) holds, we differentiate X along the solution of the model (5) to obtain:

$$\begin{aligned} \frac{dX}{dt} &= \left(1 - \frac{S^*}{S}\right)\frac{dS}{dt} + \left(1 - \frac{E^*}{E}\right)\frac{dE}{dt} + \left(1 - \frac{I_T^*}{I_T}\right)\frac{dI_T}{dt} \\ &+ \left(1 - \frac{I_C^*}{I_C}\right)\frac{dI_C}{dt} + \left(1 - \frac{I_{CT}^*}{I_{CT}}\right)\frac{dI_{CT}}{dt} + \left(1 - \frac{H^*}{H}\right)\frac{dH}{dt} \\ &+ \left(1 - \frac{R^*}{R}\right)\frac{dR}{dt} + \left(1 - \frac{B_T^*}{B_T}\right)\frac{dB_T}{dt} + \left(1 - \frac{B_C^*}{B_C}\right)\frac{dB_C}{dt}. \end{aligned} \tag{20}$$

Substituting system (5) into equation (21) yields

$$\begin{aligned} \frac{dX}{dt} =& \left(1 - \frac{S^*}{S}\right)(\alpha\, R - \lambda\, S - \mu_1 S + \Lambda) + \left(1 - \frac{E^*}{E}\right)(\lambda\, S - (\mu_1 + \tau)E) \\ &+ \left(1 - \frac{I_T^*}{I_T}\right)(\tau\, nE + \sigma\, h_1 I_{CT} - (k_1 + \Psi_1 + \mu_1 + r_1)I_T) \\ &+ \left(1 - \frac{I_C^*}{I_C}\right)(\tau\, mE + \sigma\, h_2 I_{CT} - (\mu_1 + r_3 + k_3 + \Psi_3)I_C) \\ &+ \left(1 - \frac{I_{CT}^*}{I_{CT}}\right)(m + n)\tau\, E - (\sigma\, h_1 + \sigma\, h_2 + k_2(1 - (h_1 + h_2) + \mu_1 + r_2))I_{CT}) \\ &+ \left(1 - \frac{H^*}{H}\right)(k_2(1 - (h_1 + h_2))I_{CT} + k_1 I_T + k_3 I_C - (\Psi_2 + \mu_1)H) \\ &+ \left(1 - \frac{R^*}{R}\right)(\Psi_2 H + \Psi_3 I_C + \Psi_1 I_T - (\mu_1 + \alpha)R) \end{aligned} \tag{21}$$

$$+\left(1-\frac{B_T^*}{B_T}\right)(g_T B_T(1-\frac{B_T}{K_T})+g_1 I_T+g_2 I_{CT}-\mu_3 B_T)$$
$$+\left(1-\frac{B_C^*}{B_C}\right)(g_C B_C(1-\frac{B_C}{K_C})+g_3 I_{CT}+g_4 I_C-\mu_2 B_C).$$

Now substitute

$S=S-S^*, E-E^*, I_T-I_T^*, I_C-I_C^*, I_{CT}-I_{CT}^*, H-H^*, R-R^*, B_T-B_T^*, B_C-B_C^*$, gives

$$\begin{aligned}
\frac{dX}{dt} &= \left(\frac{S-S^*}{S}\right)^2(-\lambda-\mu_1)+\Lambda\left(\frac{(S-S^*)}{S}\right)+\alpha\left(\frac{(R-R^*)(S-S^*)}{S}\right)+\lambda(S-S^*)\\
&-(\mu_1+\tau)(E-E^*)+\tau n(E-E^*)+\sigma h_1(I_{CT}-I_{CT}^*)-(k_1+\Psi_1+\mu_1+r_1)(I_T-I_T^*)\\
&+\tau m(E-E^*)+\sigma h_2(I_{CT}-I_{CT}^*)-(\mu_1+r_3+k_3+\Psi_3)(I_C-I_C^*)+(m+n)\tau(E-E^*)\\
&-(\sigma h_1+\sigma h_2+k_2(1-(h_1+h_2)+\mu_1+r_2))(I_{CT}-I_{CT}^*)+k_2(1-(h_1+h_2))(I_{CT}-I_{CT}^*)\\
&+k_1(I_T-I_T^*)+k_3(I_C-I_C^*)-(\Psi_2+\mu_1)(H-H^*)-\mu_1(R-R^*)+\Psi_2(H-H^*)+\Psi_3(I_C-I_C^*)\\
&+\Psi_1(I_T-I_T^*)+g_T(B_T-B_T^*)\left(1-\tfrac{(B_T-B_T^*)}{K_T}\right)+g_1(I_T-I_T^*)+g_2(I_{CT}-I_{CT}^*)-\mu_3(B_T-B_T^*)\\
&+g_C(B_C-B_C^*)\left(1-\tfrac{(B_C-B_C^*)}{K_T}\right)+g_3(I_{CT}-I_{CT}^*)+g_4(I_C-I_C^*)-\mu_2(B_C-B_C^*).
\end{aligned} \tag{22}$$

Now, collecting positive and negative terms together in the system (22):

$$\frac{dX}{dt} = Q-Z \tag{23}$$

Let,

$$\begin{aligned}
Q &= \Lambda\left(\frac{(S-S^*)}{S}\right)+\alpha\left(\frac{(R-R^*)(S-S^*)}{S}\right)+\lambda(S-S^*)+\tau n(E-E^*)\\
&+\sigma h_1(I_{CT}-I_{CT}^*)+\tau m(E-E^*)+\sigma h_2(I_{CT}-I_{CT}^*)+(m+n)\tau(E-E^*)\\
&+k_2(1-(h_1+h_2))(I_{CT}-I_{CT}^*)+k_1(I_T-I_T^*)+k_3(I_C-I_C^*)\\
&+\Psi_3(I_C-I_C^*)+\Psi_1(I_T-I_T^*)+g_T(B_T-B_T^*)+g_1(I_T-I_T^*)+g_2(I_{CT}-I_{CT}^*)\\
&+g_C(B_C-B_C^*)+g_4(I_C-I_C^*)+g_3(I_{CT}-I_{CT}^*).
\end{aligned} \tag{24}$$

and

$$\begin{aligned}
Z &= \left(\frac{S-S^*}{S}\right)^2(\lambda+\mu_1)+(\mu_1+\tau)(E-E^*)+(k_1+\Psi_1+\mu_1+r_1)(I_T-I_T^*)\\
&+(\mu_1+r_3+k_3+\Psi_3)(I_C-I_C^*)+(\sigma h_1+\sigma h_2+k_2(1-(h_1+h_2)+\mu_1+r_2))(I_{CT}-I_{CT}^*)\\
&+(\Psi_2+\mu_1)(H-H^*)+\mu_1(R-R^*)+g_T\tfrac{(B_T-B_T^*)^2}{K_T}+g_C\tfrac{(B_C-B_C^*)^2}{K_C}+\mu_3(B_T-B_T^*)\\
&+\mu_2(B_C-B_C^*).
\end{aligned} \tag{25}$$

Then,

$$\frac{dX}{dt} < 0 \quad \text{and only if} \tag{26}$$

$S=S^*, E=E^*, I_T=I_T^*, I_C=I_C^*, I_{CT}=I_{CT}^*, H=H^*, R=R^*, B_T=B_T^*,$ and $B_C=B_C^*$

Therefore, the maximum compact invariant set in $\{S, E, I_T, I_C, I_{CT}, H, R, B_T, B_C \in \Omega : \frac{dX}{dt} = 0\}$ is a singleton $\{E^*\}$ is the endemic equilibrium of the model system (5). Then by LaSalle's invariant principle, it implies that E^* is a globally asymptotically stable in the interior of Ω if $Q < Z$.

3.2.5. *Global Sensitivity Analysis.* The global sensitivity analysis is carried out using the Latin Hypercube Sampling and Partial Rank Correlation Coefficient PRCC [30]. This is a robust sensitivity measure that combines uncertainty analysis with a partial correlation coefficient to assess the sensitivity of outcome variables to parameter variation. A positive PRCC value denotes a positive correlation between the input parameter and the model output. On the other hand, a negative PRCC value indicates an inverse correlation between the input parameter and the model output, which means that the model output tends to increase as the input parameter value increases and to decrease when the input parameter value drops, as depicted in the following figures;

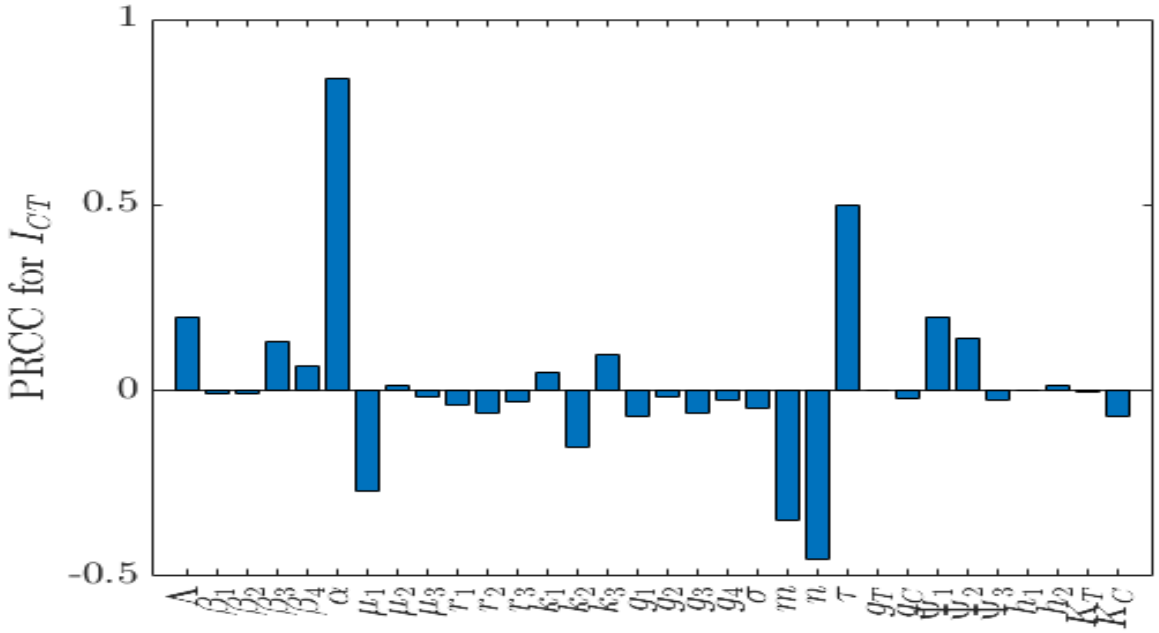

FIGURE 2. Sensitivity Analysis PRCCs of parameters with respect to co-infected individuals (I_{CT}).

Figure 2 shows the rate of loss of immunity (α) for recovered individuals, the transition rate per day to infected classes (τ), the human recruitment rate (Λ), the contact rate of COVID-19 through human-to-human transmission (β_3), the contact rate of COVID-19 environment-to-human transmission (β_4), the natural recovery rate for Typhoid fever individuals (Ψ_1) and the recovery rate of hospitalization for individual rate (Ψ_2) are positively correlated to individuals infected with both Typhoid and COVID-19 co-infections and such increase the burden of Typhoid fever and COVID-19 co-infection infection in the

human population [31]. On the other hand, the rate of screening of exposed individuals with COVID-19 (m), the natural human death rate (μ_1), the rate of screening of exposed individuals with Typhoid fever only (n), the transfer rate of individuals infected by Typhoid fever and COVID-19 (k_2) , the carrying capacity for SARS-CoV-2 virus (K_c), and the natural recovery rate of COVID-19 only (Ψ_3) are negatively correlated to Typhoid fever and COVID-19 co-infection and decrease the burden of Typhoid fever and COVID-19 co-infection infection in the human population when they are increased [32]. This implies that an increase or decrease in these parameters results in a decrease or increase in co-infection cases. The results suggest that hospitalization should be applied throughout the infection period to decrease the number of individuals infected by Typhoid fever and COVID-19.

4. Numerical Simulation of the Model

The underlying situations of SARS-Cov-2 and Salmonella Typhi in human populations are investigated numerically by solving system (5) with the parameters in Table 3, the initial conditions, given as $S(0) = 3200, E(0) = 2, I_T(0) = 0, I_C(0) = 0, I_{CT}(0) = 0, H(0) = 0, R(0) = 0, B_T(0) = 10000$ and $B_C(0) = 10000$.

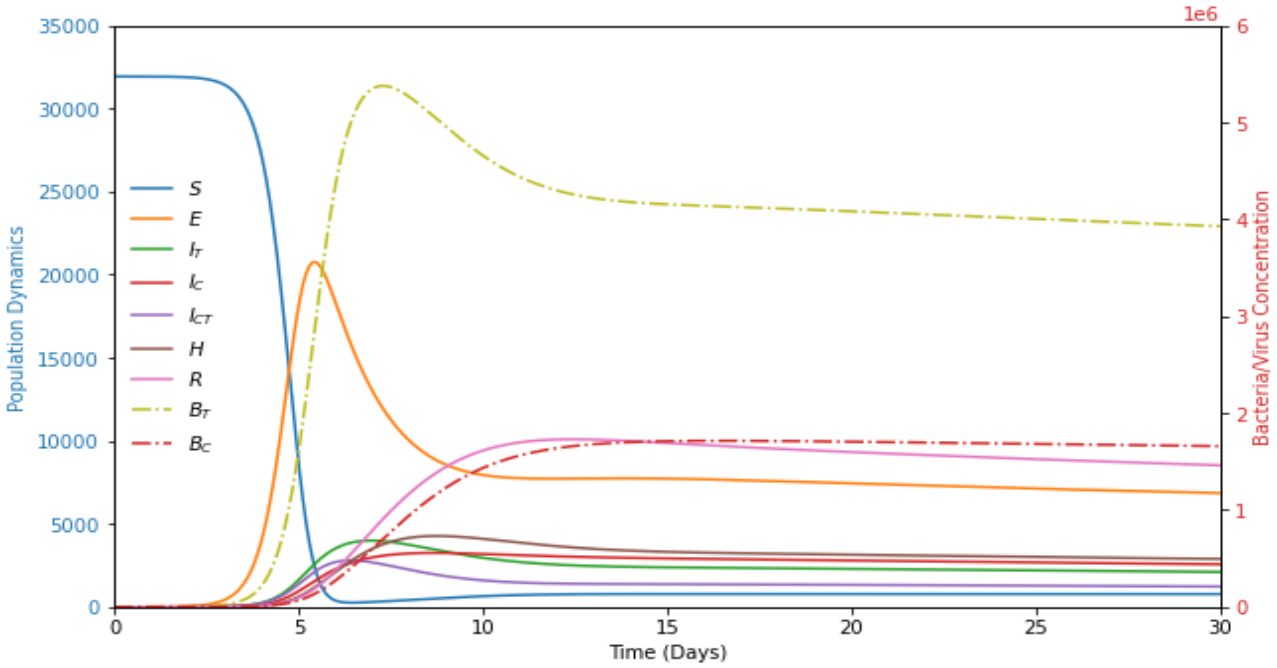

Figure 3. The plot representing the distribution of humans and pathogens population with time (days).

Figure 3 shows the distribution of different human and pathogen populations with time (days). It can be seen from Figure 3 that; the susceptible human population decreases rapidly within the first 5 days as time increases due to Salmonella typhi and SARS-Cov-2 infections and natural mortality rate.

During this stage, there are variations and adjustments in the population sizes as the disease spreads and the immune response starts to take effect. The decline of susceptible individuals does not go to zero, rather it stabilizes at 1000 due to the continuous recruitment rate and recovers individuals that lose protective immunity. Figure 3 shows that the number of infected individuals increases as time increases. Also, Figure 3 shows that the environmental pathogens increase as the number of infected individuals increases. The increase of infected individuals is caused by the increasing concentration of pathogens in the environment which is caused by the growth rates of salmonella typhi and SARS-Cov-2 and the shedding rates of the infected individuals.

4.1. **The impact of a contaminated environment on transmission of COVID-19 and Typhoid fever co-infection diseases.**

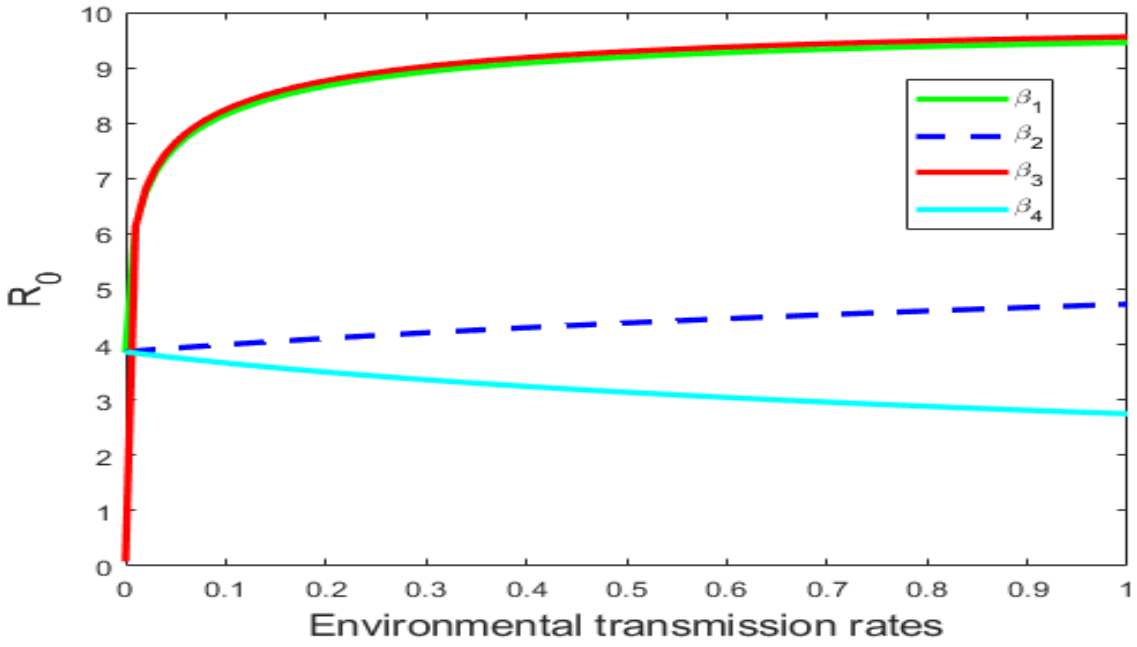

FIGURE 4. Impact of environmental factors in transmission dynamics of COVID-19 and Typhoid fever co-infection diseases.

The effect of transmission rates on $\mathcal{R}_0$ dynamics are depicted in Figure 4. In Figure 4, the variation of $\mathcal{R}_0$ for β_1, β_2, β_3 and β_4 is presented. It can be seen that when the number of transmission rates increases also the number of $\mathcal{R}_0$ increases. This indicates that higher transmission rates increase the likelihood of environmental contamination, creating opportunities for indirect or direct transmission to susceptible individuals. Furthermore, Figure 4 illustrates that the transmission coefficient of diseases in contaminated environments to susceptible individuals is more significant than other transmission rates, as evidenced by the extremely high value of $\mathcal{R}_0$ that results from an increase in its value.

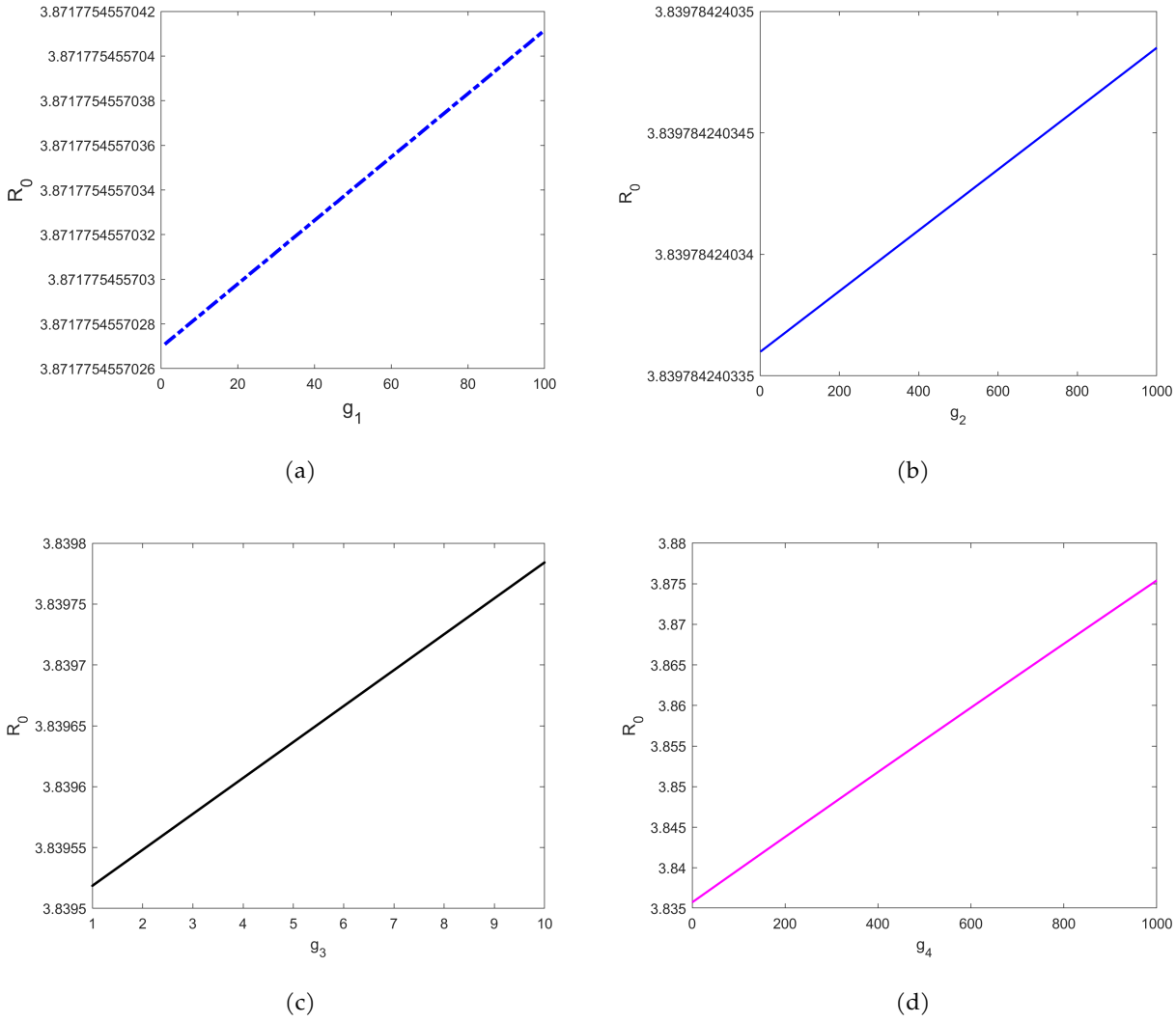

FIGURE 5. Impact of shedding rates in transmission dynamics of COVID-19 and Typhoid fever co-infection diseases

.

The effect of shedding rates on $\mathcal{R}_0$ dynamics is depicted in figure 5(a)-(d). In figure 5(a)-(d), the variation of $\mathcal{R}_0$ for $g_1, g_2, g_3,$ and g_4 is presented. It can be seen from figure 5(a)-(d) that when the number of shedding rates increases also the number of $\mathcal{R}_0$ increases. This indicates that high shedding rates increase the likelihood of environmental contamination with infectious agents, creating opportunities for indirect transmission to susceptible individuals. Consequently, this leads to an increase in the number of people infected by Typhoid fever. On the contrary, low shedding rates decrease the number of $\mathcal{R}_0$. This implies that the number of individuals infected by chance by Typhoid fever, COVID-19 and co-infection decreases.

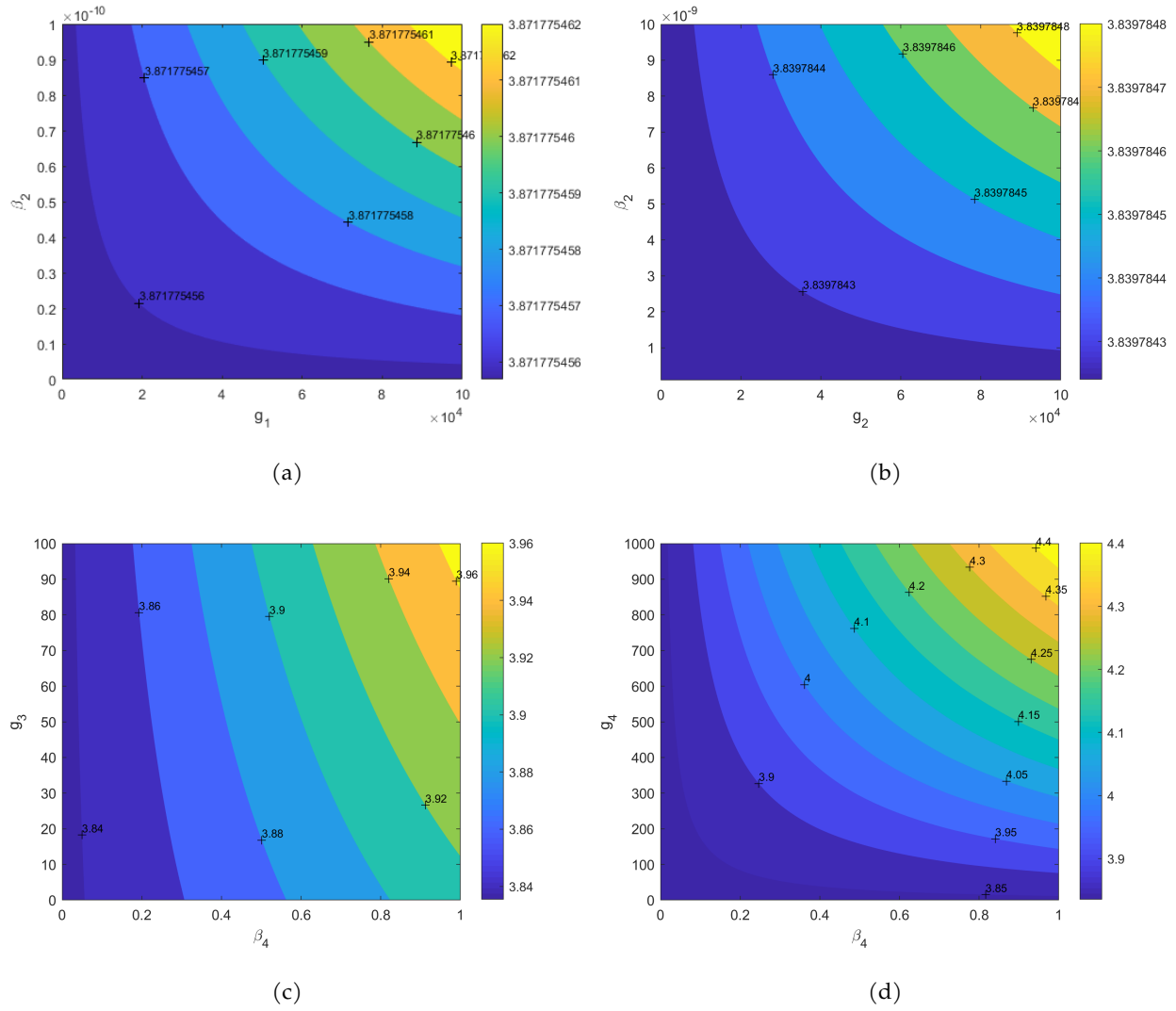

FIGURE 6. Contour plot showing the effect of shedding rates and transmission rates on $\mathcal{R}_0$.

Figure 6(a)-(d) shows the contour plots of different model parameters. It can be seen from the figures that each parameter contributes towards the dynamics of $\mathcal{R}_0$ as the changes in the values of these parameters significantly affect the value of $\mathcal{R}_0$. In figure 6(a)-(d), the variation of $\mathcal{R}_0$ for β_2 and β_4 is obtainable. It can be seen from figure 6 that β_2 and β_4 contributes towards the increasing value of $\mathcal{R}_0$, which is environment with Salmonella typhi-to-human transmission rate and environment with SARS-COV-2-to-human transmission rate. This indicates freely movement of individuals without any restriction can spread the diseases. The variation of $\mathcal{R}_0$ for β_2 and shedding rates (g_1 and g_2) is shown. From figure 6(a) and 6(b), it is clear that environmental pathogens can make the infection in the population. Similar behavior is observed from figure 6(c) and 6(d) for β_4 and shedding rates (g_3, and g_4), it is also revealed that environmental pathogens can make the infection in the population.

In contrast, the spread can be controlled by introducing effective environmental hygiene, sanitation and disinfection which reduce the transmission route of typhoid fever and COVID-19 to human population.

4.2. **Hospitalization Effect.**

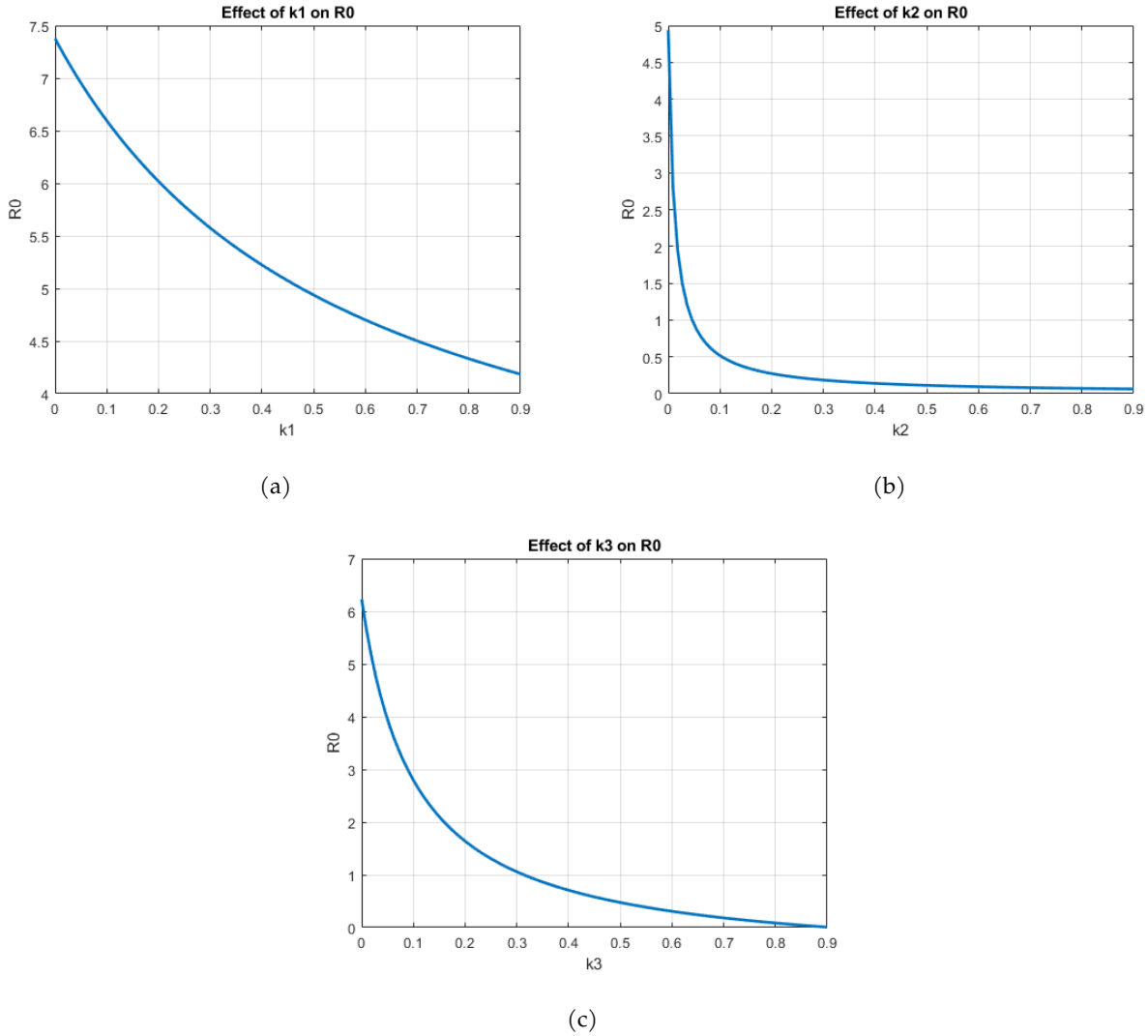

(a) (b)

(c)

FIGURE 7. Effect of Hospitalization rates on $\mathcal{R}_0$.

Figure 7(b) shows an inverse relationship between $\mathcal{R}_0$ and k_2, the result indicates that higher hospitalization rates lead to lower values of $\mathcal{R}_0$. This observation holds for k_1 and k_3 respectively. Thus, the results suggested that increasing hospitalization rates can effectively reduce the spread and impact of infectious diseases in the population.

5. Conclusion

The study proposed a mathematical model to examine the impact of contaminated environments on transmitting COVID-19 and Typhoid fever co-infections. The analysis of the model focuses on determining the local and global stability of the disease-free-equilibrium, and the basic reproduction number $\mathcal{R}_0$ using the next-generation method. The disease-free-equilibrium is locally asymptotically stable when the basic reproduction number $\mathcal{R}_0 < 1$. Additionally, a sensitivity analysis identified several important parameters that significantly impact the reproduction number, the results revealed that the rate of loss of immunity for recovered individuals (α), transition rate per day to infected classes (τ), the human recruitment rate (Λ), the contact rate of COVID-19, human-to-human (β_3), the contact rate of COVID-19 environment-to-human transmission rate (β_4), the natural recovery rate for Typhoid fever (Ψ_1) and the recovery rate due to hospitalization for individuals rate (Ψ_2). The analysis found that these parameters positively correlate with individuals infected with both Typhoid fever and COVID-19 co-infection, such increase in the burden of Typhoid fever and COVID-19 co-infection infection in the human population. On the other hand, the rate of screening of exposed individuals with COVID-19 (m), the natural human death rate (μ_1), the rate of screening of exposed individuals with Typhoid fever only (n), the transfer rate of individuals infected by Typhoid fever and COVID-19 (k_2), the carrying capacity for the SARS-CoV-2 virus (K_c), and the natural recovery rate of COVID-19 only (Ψ_3) are negatively correlated to Typhoid fever and COVID-19 co-infection and decrease the burden of Typhoid fever and COVID-19 co-infection infection in the human population. Numerical simulation shows that as the number of infected individuals increases the number of pathogens in the environment also increases. Higher transmission and shedding rates from infected individuals lead to increased environmental contamination, enabling direct and indirect transmission to susceptible individuals. Additionally, increasing the hospitalization rates for infected individuals can effectively reduce the spread and impact of infectious diseases within a community. To control the disease the reproduction number must be decreased below one. Finally, it is recommended that if the reproduction number for COVID-19 and Typhoid fever diseases is reduced below unity by decreasing the transmission and shedding rates by effective use of environmental hygiene, sanitation, and disinfection reduce typhoid fever and COVID-19 transmission from contaminated environment to human population.

TABLE 3. Model Parameter Values

Parameter	Value	Source
Λ	447	Assumed
β_1	0.0000207	[33]
β_2	1.97×10^{-11}	[34]
β_3	0.001	Assumed
β_4	0.05	Assumed
α	0.3	[35]
μ_1	0.014	[21]
μ_2	0.033	[36]
μ_3	0.119	Assumed
r_1	0.052	[37]
r_2	0.05	Assumed
r_3	0.0447	[36]
k_1	0.002	[37]
k_2	0.94	[20]
k_3	0.13978	[38]
g_1	1000	Assumed
g_2	1000	Assumed
g_3	10	[39]
g_4	100	Assumed
σ	0.2	[40]
n	0.4	Assumed
m	0.2	[41]
τ	0.43	Assumed
g_T	0.25	[42]
g_C	0.2	Assumed
Ψ_1	0.5	[3]
Ψ_2	0.5	Assumed
Ψ_3	0.043	[43]
h_1	0.005	[36]
h_2	0.04	[36]
K_T	1,000,000	[34]
K_C	1,000,000	[34]

Authors' Contributions

Daniel S. Mgonja: Developed and created the model; analyzed and interpreted the data; and wrote the manuscript. Alfred Hugo: Developed and created the model, Manuscript - review and editing, and Insightful suggestions. Asha Hassan: Developed and created the model, Manuscript - review and editing, and Insightful ideas. Oluwole Daniel Makinde: Developed and created the model; and made critical feedback.

Acknowledgement

We appreciate the support provided by the University of Dodoma and the Tanzania Institute of Accountancy .

Conflicts of Interest

The authors declare that there are no conflicts of interest regarding the publication of this paper.

References

[1] M. Kasanga, S. Mudenda, T. Gondwe, et al. Impact of COVID-19 on blood donation and transfusion services at Lusaka provincial blood transfusion centre, Zambia, Pan Afr. Med. J. 35 (2020), 74. https://doi.org/10.11604/pamj.supp.2020.35.2.23975.

[2] S. Saha, G.P. Samanta, Analysis of a COVID-19 model implementing social distancing as an optimal control strategy, in: N. Rezaei (Ed.), Integrated Science of Global Epidemics, Springer International Publishing, Cham, 2023: pp. 211–258. https://doi.org/10.1007/978-3-031-17778-1_10.

[3] H. Alfred, N.M. Laurencia, K. Raymond, Modelling transmission dynamics of coronavirus with infected immigrants in Tanzania, Afr. J. Pure Appl. Sci. 2 (2021), 118–126.

[4] N. Chen, M. Zhou, X. Dong, et al. Epidemiological and clinical characteristics of 99 cases of 2019 novel coronavirus pneumonia in Wuhan, China: a descriptive study, The Lancet 395 (2020), 507–513. https://doi.org/10.1016/s0140-6736(20)30211-7.

[5] Z.W. Baloch, S.L. Asa, J.A. Barletta, et al. Overview of the 2022 WHO classification of thyroid neoplasms, Endocr. Pathol. 33 (2022), 27–63. https://doi.org/10.1007/s12022-022-09707-3.

[6] S. Vinayagam, K. Sattu, SARS-CoV-2 and coagulation disorders in different organs, Life Sci. 260 (2020), 118431. https://doi.org/10.1016/j.lfs.2020.118431.

[7] S.I. Ayoubzadeh, S. Isabel, E.A. Coomes, et al. Enteric fever and COVID-19 co-infection in a teenager returning from Pakistan, J. Travel Med. 28 (2021), taab019. https://doi.org/10.1093/jtm/taab019.

[8] A. Abidemi, J.O. Akanni, O.D. Makinde, A non-linear mathematical model for analysing the impact of COVID-19 disease on higher education in developing countries, Healthcare Anal. 3 (2023), 100193. https://doi.org/10.1016/j.health.2023.100193.

[9] S. Mushayabasa, A simple epidemiological model for typhoid with saturated incidence rate and treatment effect, Int. J. Math. Comp. Sci. 6 (2013), 688–695.

[10] K.G. Mekonen, S.F. Balcha, L.L. Obsu, et al. Mathematical modeling and analysis of TB and COVID-19 coinfection, J. Appl. Math. 2022 (2022), 2449710. https://doi.org/10.1155/2022/2449710.

[11] K. Azuma, U. Yanagi, N. Kagi, et al. Environmental factors involved in SARS-CoV-2 transmission: effect and role of indoor environmental quality in the strategy for COVID-19 infection control, Environ. Health Prev. Med. 25 (2020), 66. https://doi.org/10.1186/s12199-020-00904-2.

[12] C. LeBoa, S. Shrestha, J. Shakya, et al. Environmental sampling for typhoidal Salmonellas in household and surface waters in Nepal identifies potential transmission pathways, PLoS Negl. Trop. Dis. 17 (2023), e0011341. https://doi.org/10.1371/journal.pntd.0011341.

[13] Sri Guru Ram Das University of Health Sciences Sri Amritsar, SARS-CoV manual, https://aomsi.com/Guidelines/SARS-CoV2%20MANUAL.pdf.

[14] D. Paul, P. Kolar, S.G. Hall, A review of the impact of environmental factors on the fate and transport of coronaviruses in aqueous environments, Npj Clean Water 4 (2021), 7. https://doi.org/10.1038/s41545-020-00096-w.

[15] M. Achak, S. Alaoui Bakri, Y. Chhiti, et al. SARS-CoV-2 in hospital wastewater during outbreak of COVID-19: A review on detection, survival and disinfection technologies, Sci. Total Environ. 761 (2021), 143192. https://doi.org/10.1016/j.scitotenv.2020.143192.

[16] H. Choi, P. Chatterjee, J.D. Coppin, et al. Current understanding of the surface contamination and contact transmission of SARS-CoV-2 in healthcare settings, Environ. Chem. Lett. 19 (2021), 1935–1944. https://doi.org/10.1007/s10311-021-01186-y.

[17] M.L. Diagne, H. Rwezaura, S.Y. Tchoumi, J.M. Tchuenche, A Mathematical Model of COVID-19 with Vaccination and Treatment, Comp. Math. Meth. Med. 2021 (2021), 1250129. https://doi.org/10.1155/2021/1250129.

[18] M. Bueckert, R. Gupta, A. Gupta, M. Garg, A. Mazumder, Infectivity of SARS-CoV-2 and other coronaviruses on dry surfaces: Potential for indirect transmission, Materials 13 (2020), 5211. https://doi.org/10.3390/ma13225211.

[19] N. Zhang, W. Chen, P. Chan, H. Yen, J.W. Tang, Y. Li, Close contact behavior in indoor environment and transmission of respiratory infection, Indoor Air 30 (2020), 645–661. https://doi.org/10.1111/ina.12673.

[20] N.I. Akinwande, T.T. Ashezua, R.I. Gweryina, et al. Mathematical model of COVID-19 transmission dynamics incorporating booster vaccine program and environmental contamination, Heliyon 8 (2022), e11513. https://doi.org/10.1016/j.heliyon.2022.e11513.

[21] M.A. Stephano, J.I. Irunde, J.A. Mwasunda, C.S. Chacha, A continuous time Markov chain model for the dynamics of bovine tuberculosis in humans and cattle, Ricerche Mat. (2022). https://doi.org/10.1007/s11587-022-00696-3.

[22] A.G. Wedajo, B.K. Bole, P.R. Koya, Analysis of SIR mathematical model for malaria disease with the inclusion of infected immigrants, IOSR J. Math. 14 (2018), 10–21.

[23] G. Birkhoff, G.C. Rota, Ordinary differential equations, 4th ed, Wiley, New York, 1989.

[24] P. Fine, K. Eames, D.L. Heymann, "Herd immunity": A rough guide, Clin. Infect. Dis. 52 (2011), 911–916. https://doi.org/10.1093/cid/cir007.

[25] M. Bani-Yaghoub, R. Gautam, Z. Shuai, P. van den Driessche, R. Ivanek, Reproduction numbers for infections with free-living pathogens growing in the environment, J. Biol. Dyn. 6 (2012), 923–940. https://doi.org/10.1080/17513758.2012.693206.

[26] J.B.H. Njagarah, F. Nyabadza, Modelling optimal control of cholera in communities linked by migration, Comp. Math. Meth. Med. 2015 (2015), 898264. https://doi.org/10.1155/2015/898264.

[27] J.B.H. Njagarah, F. Nyabadza, Modelling optimal control of cholera in communities linked by migration, Comp. Math. Meth. Med. 2015 (2015), 898264. https://doi.org/10.1155/2015/898264.

[28] A. Mhlanga, T.V. Mupedza, A patchy theoretical model for the transmission dynamics of SARS-Cov-2 with optimal control, Sci. Rep. 12 (2022), 17840. https://doi.org/10.1038/s41598-022-21553-1.

[29] P. van den Driessche, A.A. Yakubu, Disease extinction versus persistence in discrete-time epidemic models, Bull. Math. Biol. 81 (2018), 4412–4446. https://doi.org/10.1007/s11538-018-0426-2.

[30] B. Gomero, Latin hypercube sampling and partial rank correlation coefficient analysis applied to an optimal control problem, Master's Thesis, University of Tennessee, 2012. https://trace.tennessee.edu/utk_gradthes/1278.

[31] S. Marino, I.B. Hogue, C.J. Ray, D.E. Kirschner, A methodology for performing global uncertainty and sensitivity analysis in systems biology, J. Theor. Biol. 254 (2008), 178–196. https://doi.org/10.1016/j.jtbi.2008.04.011.

[32] L. Collineau, C. Phillips, B. Chapman, et al. A within-flock model of Salmonella Heidelberg transmission in broiler chickens, Prev. Vet. Med. 174 (2020), 104823. https://doi.org/10.1016/j.prevetmed.2019.104823.

[33] L. Qin, S.X. Yang, M.Q.H. Meng, A mathematical model with degree of risk for Salmonella infections, in: 2007 IEEE International Conference on Systems, Man and Cybernetics, IEEE, Montreal, QC, Canada, 2007: pp. 2704–2709. https://doi.org/10.1109/ICSMC.2007.4413891.

[34] L. Matsebula, F. Nyabadza, Mathematical analysis of cholera typhoid co-infection transmission dynamics, Front. Appl. Math. Stat. 8 (2022), 892098. https://doi.org/10.3389/fams.2022.892098.

[35] S. Edward, N. Nyerere, Modelling typhoid fever with education, vaccination and treatment, Eng. Math. 1 (2016), 44–52.

[36] I.M. Hezam, A. Foul, A. Alrasheedi, A dynamic optimal control model for COVID-19 and cholera co-infection in Yemen, Adv. Differ. Equ. 2021 (2021), 108. https://doi.org/10.1186/s13662-021-03271-6.

[37] G.T. Tilahun, O.D. Makinde, D. Malonza, Modelling and optimal control of typhoid fever disease with cost-effective strategies, Comp. Math. Meth. Med. 2017 (2017), 2324518. https://doi.org/10.1155/2017/2324518.

[38] A. Omame, H. Rwezaura, M.L. Diagne, S.C. Inyama, J.M. Tchuenche, COVID-19 and dengue co-infection in Brazil: optimal control and cost-effectiveness analysis, Eur. Phys. J. Plus 136 (2021), 1090. https://doi.org/10.1140/epjp/s13360-021-02030-6.

[39] M. Srinivasan, K.N. Sindhu, S. Giri, et al. Salmonella typhi shedding and household transmission by children with blood culture-confirmed typhoid fever in Vellore, South India, J. Infect. Dis. 224 (2021), S593–S600. https://doi.org/10.1093/infdis/jiab409.

[40] S. Nawaz, M. Saleem, COVID-19 and coinfections: A serious health threat requires combination of diagnosis and therapy, Infect. Disord. Drug Targets 22 (2022), 7–13. https://doi.org/10.2174/1871526522666220407001744.

[41] A. Atkeson, M. Droste, M. Mina, J. Stock, Economic benefits of COVID-19 screening tests, National Bureau of Economic Research, Cambridge, MA, 2020. https://doi.org/10.3386/w28031.

[42] L.I. Syarif, A.R. Junita, M. Hatta, A mini review: Medicinal plants for typhoid fever in Indonesia, Syst. Rev. Pharm. 11 (2020), 1171–1180.

[43] I.I. Oke, Y.T. Oyebo, O.F. Fakoya, V.S. Benson, Y.T. Tunde, A mathematical model for Covid-19 disease transmission dynamics with impact of saturated treatment: Modeling, analysis and simulation, Open Access Libr. J. 08 (2021), 1–20. https://doi.org/10.4236/oalib.1107332.